

# Measuring supermassive black holes with gas kinematics: the active S0 galaxy NGC 3998<sup>★,★★</sup>

Giovanna De Francesco<sup>1</sup>, Alessandro Capetti<sup>1</sup>, and Alessandro Marconi<sup>2</sup>

<sup>1</sup> INAF - Osservatorio Astronomico di Torino, Strada Osservatorio 20, I-10025 Pino Torinese, Italy  
e-mail: defrancesco@to.astro.it, capetti@to.astro.it

<sup>2</sup> INAF - Osservatorio Astrofisico di Arcetri Largo E. Fermi 5, I-50125 Firenze, Italy  
e-mail: marconi@arcetri.astro.it

Received / Accepted

## ABSTRACT

*Context.* We present results from a kinematical study of the gas in the nucleus of the active S0 galaxy NGC 3998 obtained from archival HST/STIS long-slit spectra.

*Aims.* We analyzed the emission lines profiles and derived the map of the gas velocity field. The observed velocity curves are consistent with gas in regular rotation around the galaxy's center.

*Methods.* By modeling the surface brightness distribution and rotation curve of the H $\alpha$  emission line we found that the observed kinematics of the circumnuclear gas can be accurately reproduced by adding to the stellar mass component a compact dark mass (black hole) of  $M_{\text{BH}} = 2.7^{+2.4}_{-2.0} \times 10^8 M_{\odot}$  (uncertainties at a  $2\sigma$  level); the radius of its sphere of influence ( $R_{\text{sph}} \sim 0.16$ ) is well resolved at the HST resolution.

*Results.* The BH mass estimate in NGC 3998 is in good agreement with both the  $M_{\text{BH}} - M_{\text{bul}}$  (with an upward scatter by a factor of  $\sim 2$ ) and  $M_{\text{BH}} - \sigma$  correlations (with a downward scatter by a factor of  $\sim 3 - 7$ , depending on the form adopted for the dependence of  $M_{\text{BH}}$  on  $\sigma$ ).

*Conclusions.* Although NGC 3998 cannot be considered as an outlier, its location with respect to the  $M_{\text{BH}} - \sigma$  relation conforms with the trend suggesting the presence of a connection between the *residuals* from the  $M_{\text{BH}} - \sigma$  correlation and the galaxy's effective radius. In fact, NGC 3998 has one of the smallest values of  $R_e$  among the galaxies with measured  $M_{\text{BH}}$  (0.85 kpc) and it shows a negative residual. This suggests that a combination of both  $\sigma$  and  $R_e$  is necessary to drive the correlations between  $M_{\text{BH}}$  and other bulge properties, an indication for the presence of a black holes "fundamental plane".

**Key words.** black hole physics – galaxies: active – galaxies: bulges – galaxies: nuclei – galaxies: kinematics and dynamics

## 1. Introduction

It is generally believed that supermassive black holes (SMBHs;  $\sim 10^6 - 10^{10} M_{\odot}$ ) are a common, if not universal, feature in the nuclei of nearby galaxies. Since the discovery of quasars (Schmidt 1963), it has been suggested that active galactic nuclei (AGNs) are powered by mass accretion onto a SMBH (Salpeter 1964; Lynden-Bell 1969). This belief, combined with the observed evolution of the space density of AGNs and the high incidence of low-luminosity AGN-like activity in the nucleus of nearby galaxies (Heckman 1980; Maoz et al. 1995; Ho et al. 1997a,b; Braatz et al. 1997; Barth et al. 1998, 1999; Nagar et al. 2002) implies that a significant fraction of galaxies in the Local Universe must host black holes (BHs), relics of past activity (Soltan 1982; Chokshi & Turner 1992; Yu & Tremaine 2002; Marconi et al. 2004; Shankar et al. 2004).

Supports to these beliefs came from studies of the centers of nearby early-type galaxies, which revealed that most contain SMBHs (Kormendy & Gebhardt 2001; Merritt & Ferrarese

2001) and that the BH mass  $M_{\text{BH}}$  correlates with some properties of the host galaxy, such as bulge luminosity  $L_{\text{bul}}$  and mass  $M_{\text{bul}}$  (Kormendy & Richstone 1995; Magorrian et al. 1998; Marconi & Hunt 2003), light concentration (Graham et al. 2001) and bulge velocity dispersion  $\sigma_{\text{bul}}$  (Ferrarese & Merritt 2000; Gebhardt et al. 2000; Tremaine et al. 2002). The correlation with the bulge velocity dispersion was thought to be the tightest having the smallest scatter: rms  $\sim 0.3$  in  $\log M_{\text{BH}}$ . Ferrarese & Merritt (2000) argued that, for their selected sample of 12 galaxies, thought to have the most reliable BH mass estimates, the observed scatter in the  $M_{\text{BH}} - \sigma_{\text{bul}}$  relation was fully accounted for by the assumed measurement errors, which implies that there may be no intrinsic scatter in the correlation. More recently, Marconi & Hunt (2003) have shown that when considering only galaxies with secure BH mass and bulge parameters determinations all the above correlations have a similar observed scatter (see also McLure & Dunlop 2002; Erwin et al. 2004; Häring & Rix 2004).

The existence of any intrinsic correlations of  $M_{\text{BH}}$  and host galaxy bulge properties supports the idea that the growth of SMBHs and the formation of bulges are closely linked (Silk & Rees 1998; Haehnelt & Kauffmann 2000), therefore having important implications for theories of galaxy formation and evolution. Moreover, SMBH mass estimates inferred via the above correlations, when more direct methods are unplayable, enter in a variety of important studies spanning from AGNs

Send offprint requests to: G. De Francesco

<sup>★</sup> Based on observations obtained at the Space Telescope Science Institute, which is operated by the Association of Universities for Research in Astronomy, Incorporated, under NASA contract NAS 5-26555.

<sup>★★</sup> This publication makes use of the HyperLeda database, available at <http://leda.univ-lyon1.fr>.

physics and fueling to coeval formation and evolution of the host galaxy and its nuclear black hole. These correlations need, however, to be further investigated by increasing the number of accurate BH mass determinations in nearby galactic nuclei to set these correlations on stronger statistical basis. In particular such a study has the potential to establish the precise role of the various host galaxy’s parameters in setting the resulting BH mass. To date, reliable SMBH detections have been obtained for a limited number of galaxies ( $\sim 30$ , see Ferrarese & Ford 2005 for a review), with a bulk of  $M_{\text{BH}}$  estimates in the range of  $10^7 - 10^9 M_{\odot}$ . Furthermore, the coverage of the mass range is particularly poor at the low-mass end, the sample being strongly biased against late Hubble types and low luminosity objects. To add reliable new points to the  $M_{\text{BH}}$ – host galaxy properties planes is then a fundamental task for future developments of astronomical and physical studies, and is the aim of the work described in this paper.

Spectral information at the highest possible angular resolution is required to directly measure the mass of SMBHs: the radius of the “sphere of influence” (Bahcall & Wolf 1976) of massive BHs is typically  $\lesssim 1''$  even in the nearest galaxies. Among the so far most widely used techniques to detect and estimate BHs masses is stellar dynamical modeling (e.g. Dressler & Richstone 1988; Kormendy & Richstone 1995; van der Marel et al. 1998; Gebhardt et al. 2000; Verolme et al. 2002), but the interpretation of the data is complex involving many degrees of freedom and requiring data of very high signal-to-noise ratio (Valluri et al. 2004). Radio frequency measurements of  $\text{H}_2\text{O}$  masers in disks around BHs, finally, can be applied only to the small fraction of the disks inclined such that their maser emission is directed toward us (Braatz et al. 1997). A more widely applicable and relatively simple method to detect BHs is based on gas kinematics (e.g. Harms et al. 1994; Ferrarese et al. 1996; Macchetto et al. 1997; Barth et al. 2001), through studies of ordinary optical emission lines from circumnuclear gas disks, provided that the gas velocity field is not dominated by non gravitational motions. A successful modeling of the gas velocity field under the sole influence of the stellar and black hole potential is needed to provide *a posteriori* support for a purely gravitational kinematics. The angular resolution of  $\sim 0'.1$  of the Space Telescope Imaging Spectrograph (STIS) onboard *HST* is the most suitable to perform such studies. The wealth of unpublished data contained in STIS archives represents an extraordinary and still unexplored resource.

Following this chain of reasoning, we performed a systematic search for unpublished data in the *HST* STIS archive with the aim of finding galaxies candidates to provide a successful SMBH mass measurement.

In this paper we present the results obtained for the active galaxy NGC 3998. From the Lyon/Meudon Extragalactic Database (HyperLeda), NGC 3998 is classified as an early type (S0) galaxy with a heliocentric radial velocity of  $1040 \pm 18 \text{ km s}^{-1}$ . With  $H_0 = 75 \text{ km s}^{-1} \text{ Mpc}^{-1}$  and after correction for Local Group infall onto Virgo, this corresponds to a distance of 17 Mpc and a scale of  $83 \text{ pc arcsec}^{-1}$ . NGC 3998 is spectroscopically classified as a LINER with broad  $\text{H}\alpha$  emission (Heckman 1980; Keel 1983; Ho et al. 1997a,b) and no significant broad-line polarization (Barth et al. 1999) therefore indicating a probable direct view to a BLR. Support to this hypothesis comes from studies of *HST* WFPC2 optical images which revealed an unobscured nucleus and the presence of a bright circumnuclear ionized gas disk (Pogge et al. 2000). The nucleus contains a variable compact flat spectrum radio source (Hummel et al. 1984) dis-

playing a weak jet-like northern structure (Filho et al. 2002). A bright UV source (unresolved at *HST* FOC resolution) is present in the center of NGC 3998 (Fabbiano et al. 1994). Its rapidly variable flux (Maoz et al. 2005) implies that a significant fraction of the UV output is contributed by a non-stellar AGN component. A substantial featureless continuum component is also observed in the optical (González Delgado et al. 2004). The presence of an AGN in the nucleus of NGC 3998 is further strengthened by X-ray observations, which revealed the presence of a nuclear source with a power law spectrum (Roberts & Warwick 2000; Pellegrini et al. 2000) and X-ray and  $\text{H}\alpha$  luminosity values consistent with the low luminosities extension of the correlation observed for Seyferts and QSOs (see Koratkar et al. 1995).

The paper is organized as follows: in Sec. 2 we present *HST*/STIS data and the reduction that lead to the results described in Sec. 3. In Sec. 4 we model the observed  $\text{H}\alpha$  emission line rotation curve and we show that the dynamics of the circumnuclear gas can be accurately reproduced by circular motions in a disk when a point-like dark mass is added to the stellar potential. Our results are discussed in Sec. 5, and summarized in Sec. 6.

## 2. HST data and reduction

NGC 3998 was observed with STIS on *HST* in 1997 November 01 with the G750M grating and the  $52'' \times 0'.1$  slit. Data were acquired at five different slit positions, following a perpendicular-to-slit pattern with a step of  $0'.1$  and the central slit centered on the nucleus. The orientation of the slit was  $-81^\circ$  from North, and the exposure time was 328 s for each position. The position of the continuum peak had been acquired with the ACQ mode with two 10 s exposures obtained with the optical long-pass filter MIRVIS. The five spectra obtained, NUC for the nuclear slit, N1-N2 and S1-S2 (from North to South) for the four off-nuclear, were retrieved from the public archive. Fig. 1 shows the slit locations superposed onto a narrow band WFPC2, obtained by using the F658N filter, including the  $\text{H}\alpha$ + [N II] lines.

The data were obtained with a  $2 \times 1$  on-chip binning of the detector pixels and automatically processed through the standard *CALSTIS* pipeline to perform the steps of bias and dark subtraction, applying the flat field and combining the two sub-exposures to reject cosmic-ray events. The data were then wavelength and flux calibrated with conversion to heliocentric wavelengths and absolute flux units and rectified for the geometric distortions. The 2-D spectral image obtained for each slit position has a spatial scale of  $0'.0507 \text{ pixel}^{-1}$  along the slit, a dispersion of  $\Delta\lambda = 1.108 \text{ \AA pixel}^{-1}$  and a spectral resolution of  $\mathcal{R} \approx 3000$ , covering the rest frame wavelength range 6480-7050  $\text{\AA}$ .

For each spectrum we selected the regions containing the lines of interest. The lines were fitted, row by row, along the dispersion direction, together with a linear continuum, with Gaussian functions using the task SPECFIT in STSDAS/IRAF. All emission lines present in the spectra ( $\text{H}\alpha$ , [NII] $\lambda\lambda 6548, 6583$  and [SII] $\lambda\lambda 6716, 6731$ ) were fitted simultaneously with the same velocity and width and with the relative flux of the [NII] lines kept fixed to 0.334. Results of the fit are tabulated in Appendix A.

A single Gaussian function for  $\text{H}\alpha$  line does not produce an accurate fit to the lines profile in the region  $r < 0'.2$  for three positions of the slit: NUC and the nearest N1 and S1. Here the lines profile shows a broad base component superposed to the narrow lines of  $\text{H}\alpha$  and [N II] (see Fig. 2 for NUC slit), indicative of the presence of a Broad Line Region. In these regions we performed

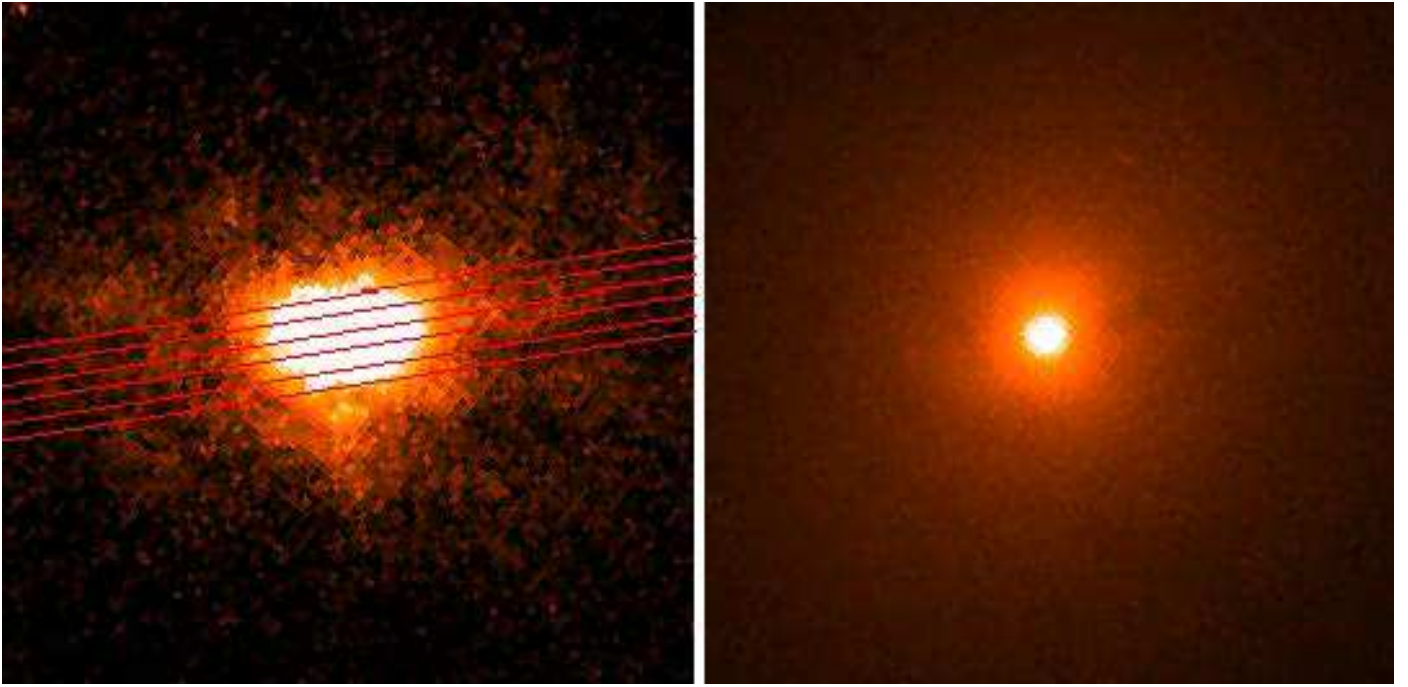


**Fig. 1.** Left)  $H\alpha$  image of the central  $4'' \times 4''$  of NGC 3998 with superposed the 5 slit locations. Right) V band (F547M filter) WFPC2/HST image of NGC 3998. North is up, East is left.

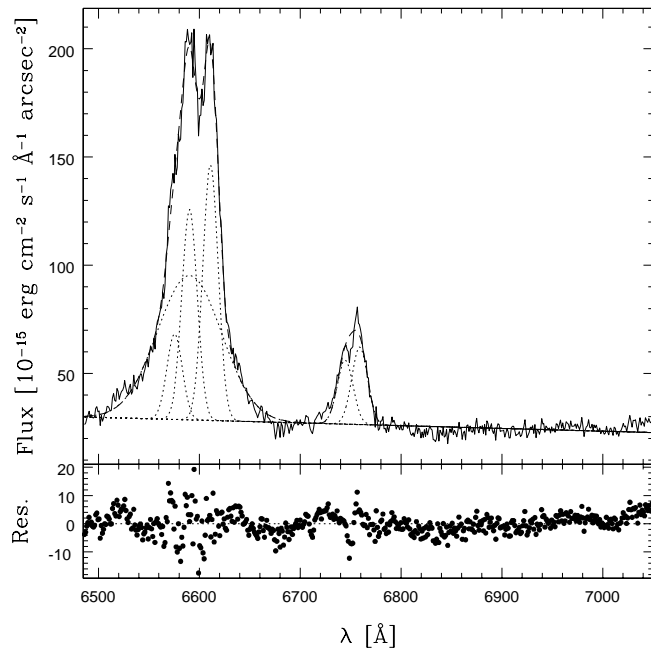


**Fig. 2.** Nuclear spectrum of NGC 3998 showing the presence of a broad  $H\alpha$  component. The best model spectrum (dashed line) is superposed to the data; dotted lines are for the gaussians and linear continuum components of the fit. The residuals from the fit are shown in the lower panel.

a fit with two Gaussians components for  $H\alpha$  line, a narrow and a broad one whose velocity we kept fixed at all locations.

In the external regions, where the SNR was insufficient the fitting was improved by co-adding two or more pixels along the slit direction.

### 3. Results

The results obtained from the fitting procedure at the five slit positions are shown in Fig. 3 through Fig. 5 where we show the central velocity, surface brightness and FWHM for the narrow  $H\alpha$  line at each location along the slits. Emission is detected out to a radius of  $\sim 0'.5$  corresponding to  $\sim 40$  pc. The extension of the line emission and its behaviour along the five slit positions are in agreement with the  $H\alpha$  image seen in Fig. 1, where an  $\sim$  EST-WEST elongated emission structure is visible. Conversely, the stellar component shows an almost circular distribution in the V band continuum.

The line emission is strongly peaked on the central slit (Fig. 3, middle panel), rapidly decreasing at larger radii and not showing the presence of any emission line knot other than the central maximum. The velocity curve in the central slit, NUC, has a full amplitude of  $\sim 400$   $\text{km s}^{-1}$  and shows a general reflection symmetry: starting from the center the velocity rapidly rises on both sides by  $\sim 200$   $\text{km s}^{-1}$  reaching a peak at  $r \sim 0'.1$  from the center. At larger radii, the velocity decreases to form a plateau before rising again at the extremes of the velocity field. Both the line flux and the line width rapidly decrease from the nucleus outwards.

The behaviour seen in the off-nuclear slits is qualitatively similar to that seen at the NUC location, but with substantially smaller velocity amplitude and, more important, a less extreme nuclear gradient. Both amplitude and gradient decrease at increasing distance of the slit center from the nucleus, with a behaviour characteristic of gas rotating in a circumnuclear disk.

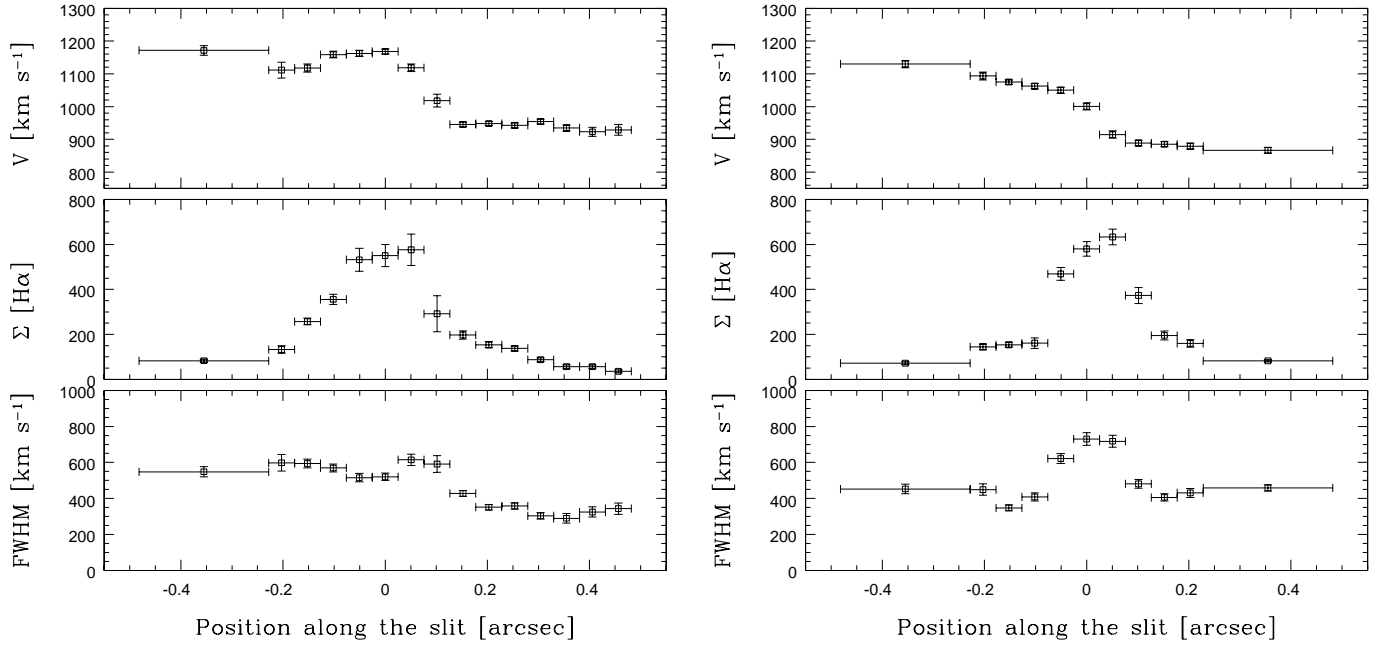


**Fig. 4.** Same as Fig. 3 for the nearest nucleus slit positions N1 (left panel) and S1 (right). In the region  $r < 0''.2$  fits are performed with a double Gaussian for H $\alpha$  line to separate the broad and narrow components.

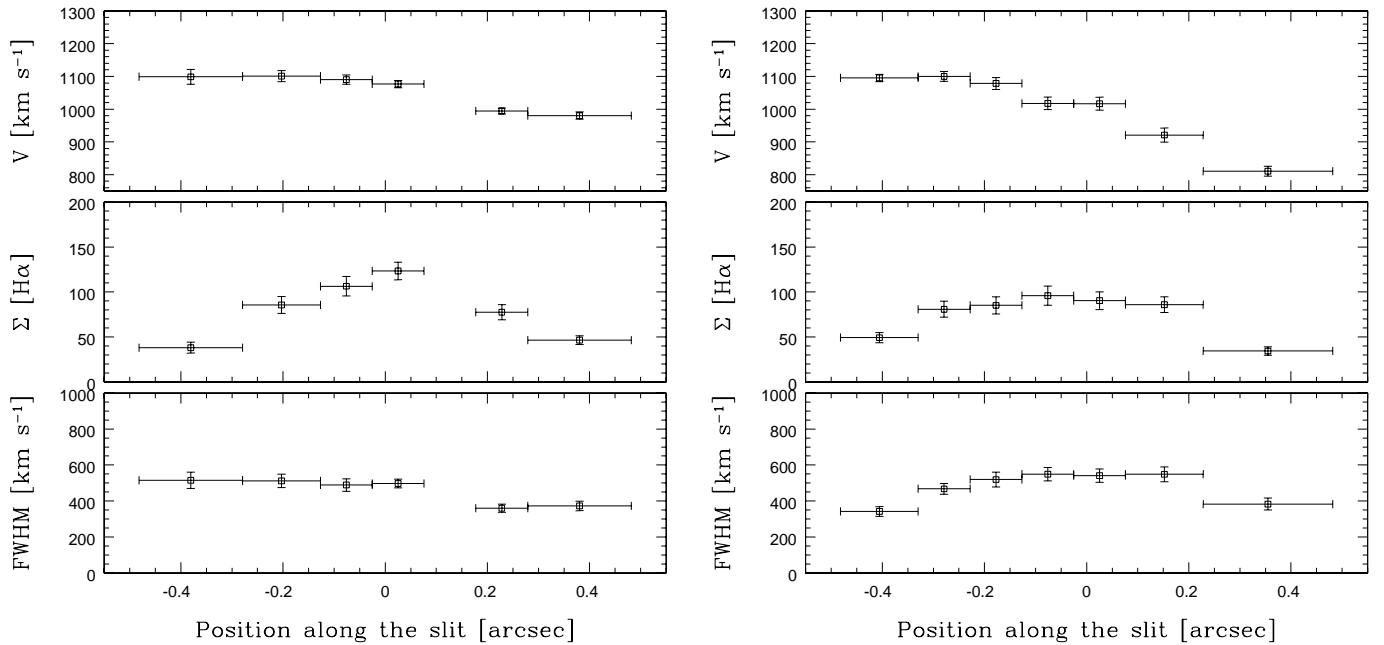


**Fig. 5.** Same as Fig. 3 for the N2 (left panel) and S2 (right) slit.

#### 4. Modeling the rotation curves

It therefore appears that an ionized gas system is present in the innermost regions of NGC 3998 with a smooth and regular velocity field, co-rotating with respect to the larger scale stellar and gas disk (Fisher 1997).

Our modeling code, described in detail in Marconi et al. (2003), was used to fit the observed rotation curves. The code computes the rotation curves of the gas assuming that the gas is rotating in circular orbits within a thin disk in the galaxy potential. The gravitational potential has two components: the stellar potential (determined in the next section), characterized by

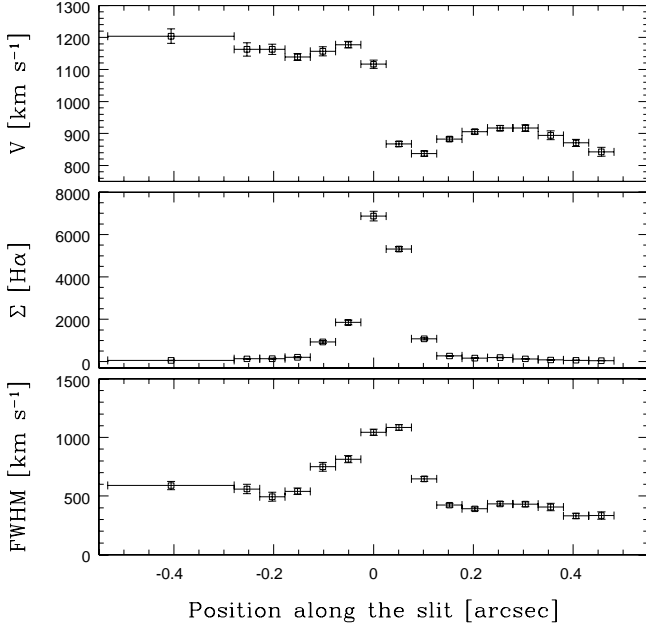


**Fig. 3.** Velocity, surface brightness and FWHM for the narrow H $\alpha$  component along the NUC slit. Surface brightness is in units of  $10^{-15}$  erg s $^{-1}$  cm $^{-2}$  arcsec $^{-2}$ . Positions along the slit are relative to the continuum peak, positive values are NW. In the region  $r < 0''.2$  fits are performed with a double Gaussian for H $\alpha$  line to separate the broad and narrow components.

its mass-to-light ratio and a dark mass concentration (the black hole), spatially unresolved at HST+STIS resolution and characterized by its total mass  $M_{\text{BH}}$ . In computing the rotation curves we take into account the finite spatial resolution of HST+STIS, the line surface brightness distribution and we integrate over the slit and pixel area. The  $\chi^2$  is minimized to determine the free parameters using the downhill simplex algorithm by Press et al. (1992).

#### 4.1. The stellar mass distribution

In order to assess the contribution of stars to the gravitational potential in the nuclear region, we derived the stellar luminosity density from the observed surface brightness distribution.

We reconstructed the galaxy light profile using a WFPC2 F547M (V band) image retrieved from the public archive (Fig. 1). An inspection of *HST* archive images shows that contamination from dust is negligible, since dust absorption is seen only on relatively large scale ( $r > 2$  kpc) while the central regions are apparently free from dust (see also Pogge et al. 2000). We used the IRAF/STSDAS program ELLIPSE to fit elliptical isophotes to the galaxy (see Fig. 6). Excluding the nuclear regions ( $r \leq 0''.15$ ) that are dominated by a central compact source, the ellipticity shows small variations around a value of  $\sim 0.15$ . The position angle does not show significant variations being approximately constant at PA = 135 $^\circ$ .

The nature of the compact nuclear source is crucial for the estimate of the stellar mass distribution. In fact, if this is associated to light produced by the active nucleus, it does not correspond to a stellar mass contribution and should not be included in the mass budget. The presence of a bright (and variable) UV

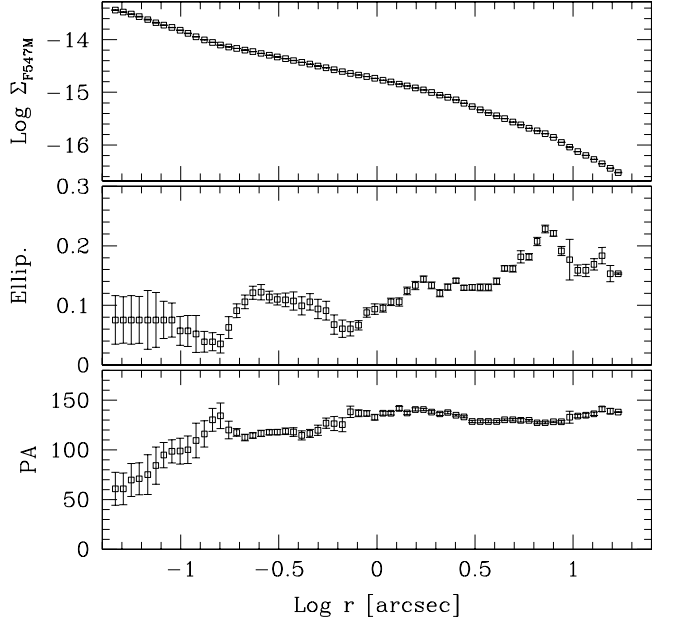


**Fig. 6.** Results of the isophotes analysis of the V band image of NGC 3998. Surface brightness is shown in the top panel (in units of erg s $^{-1}$  cm $^{-2}$  Å $^{-1}$  arcsec $^{-2}$ ), the galaxy's ellipticity and position angle are shown in the middle and bottom panels respectively.

and X-ray source seems to indicate that indeed this is the case. We explored in more detail this issue by fitting the brightness profile with a Sérsic law (Sérsic 1968) with superposed a point source, whose profile was derived from a synthetic Point Spread Function modeled with TINYTIM. This analysis shows a very good agreement between the data and the model (see Fig. 7). This supports the conclusion that the central source is unresolved and associated to AGN emission.

The inversion procedure to derive the stars distribution from the surface brightness is not unique if the gravitational potential does not have a spherical symmetry. Assuming that the gravitational potential is an oblate spheroid, the inversion depends on the knowledge of the potential axial ratio  $q$ , and the inclination of its principal plane with respect to the line of sight. As these two quantities are related by the observed isophote ellipticity, we are left with the freedom of assuming different galaxy inclinations to the line of sight. We performed the de-projection adopting for the galaxy inclination the value  $i = 40^\circ$ , as given from the HyperLeda database. Due to the small ellipticity of this galaxy, the precise value of its inclination has only a marginal effect on the resulting mass distribution.

Following van der Marel & van den Bosch (1998), we assumed an oblate spheroid density distribution parameterized as:

$$\rho(m) = \rho_0 \left( \frac{m}{r_b} \right)^{-\alpha} \left[ 1 + \left( \frac{m}{r_b} \right)^2 \right]^{-\beta}$$

where  $m$  is given by  $m^2 = x^2 + y^2 + z^2/q^2$ ,  $xyz$  is a reference system with the  $xy$  plane corresponding to the principal plane of the potential and  $q$  is the intrinsic axial ratio, and performed the de-projection adopting for the mass-to-light ratio in the V band the reference value of  $\Upsilon_V = 1$ . A detailed description of

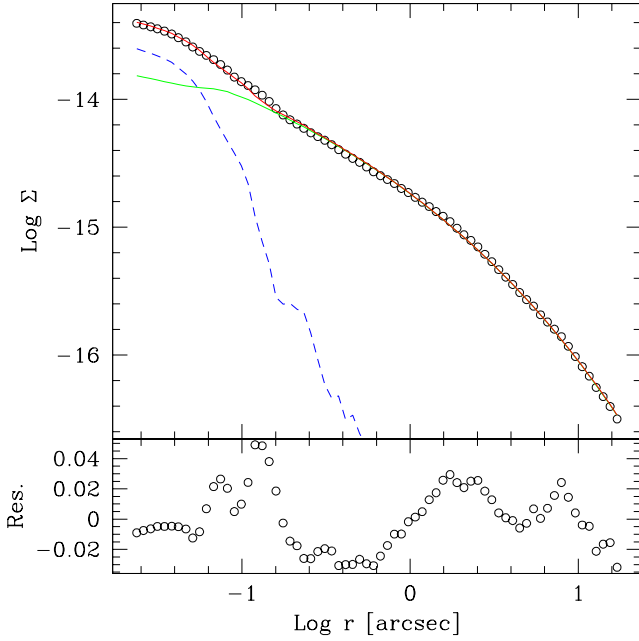


**Fig. 7.** Fit to the brightness profile of NGC 3998 obtained with a Sérsic law with an added nuclear point source (dashed line). The residuals from the fit are shown in the lower panel.

the relevant formulas and of the inversion and fit procedure is presented in Marconi et al. (2003). The best fit obtained is shown in Fig. 8 with  $\alpha = 1.67$ ,  $\beta=0.65$  and  $r_b = 4.65''^1$ . A point source with flux  $5.2 \cdot 10^{-16} \text{ erg s}^{-1} \text{ cm}^{-2} \text{ \AA}^{-1}$  was added to the extended luminosity distribution.

#### 4.2. Fitting the gas kinematics

Our modeling code was used to fit the nuclear rotation curves. The free parameters of the fit are:

- the systemic velocity,  $v_{\text{sys}}$ ,
- the impact parameter (i.e. the distance between the nuclear slit center and the center of rotation)  $b$ ,
- the position of the galaxy center along the nuclear slit  $s_0$ ,
- the angle between the slits and the line of nodes,  $\theta$ ,
- the disk inclination  $i$ ,
- the mass-to-light ratio of the stellar component,  $\mathcal{T}_V$ ,
- the black hole mass  $M_{\text{BH}}$ .

In an oblate spheroid, the stable orbits of the gas are coplanar with the principal plane of the potential and it is possible to directly associate the galaxy inclination and line of nodes with those of the circumnuclear gas. However, the potential shape is not sufficiently well determined by the isophotal fitting down to the innermost regions of the galaxy and it is possible that a change of principal plane might occur at the smallest radii, in particular within the sphere of influence of a supermassive black hole. By these considerations we preferred to leave the disk inclination as a free parameter of the fit. We then performed a  $\chi^2$

<sup>1</sup> Note that with the derived density profile, the stellar mass included within the HST spatial resolution ( $0''.1$ ) is  $4.0 \times 10^7 M_{\odot}$ , having adopted a mass-to-light ratio  $\mathcal{T}_V = 6.5$  that will be derived in the next Section. Thus it only represents a fraction of  $\sim 15\%$  of the best fit value for the SMBH mass.

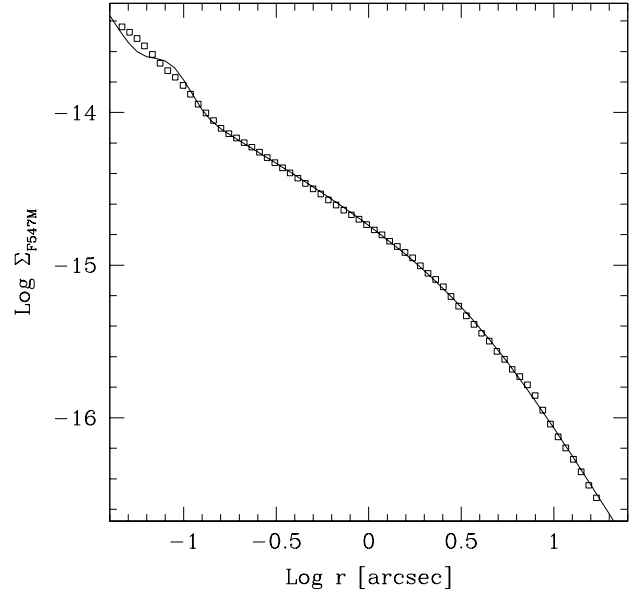


**Fig. 8.** Fit to the surface brightness profile obtained from an oblate spheroid stellar density distribution with an added nuclear point source.

minimization for different values of  $i$ , namely  $i = 10^\circ, \dots, 80^\circ$ , allowing all other parameters to vary freely. Due to the sensitivity of the observed line width to the brightness distribution modeling and to other computational problems (i.e. a coarse sampling, Marconi et al. 2006) we decided to initially perform the fit without using the values of the line width. We will show in Sect. 4.2.1 that the inclusion of the line widths in the modeling code has only a marginal effect on our results.

To build the synthetic kinematical models the intrinsic line surface brightness distribution for the narrow H $\alpha$  line had to be obtained for each disk inclination. The observed emission line surface brightness was modeled for each  $i$  value with a composition of three circularly symmetric Gaussian functions. The first reproducing the observed central emission peak, the second the intermediate regions and the third to account for the brightness behaviour at large radii. The modeling was performed through a  $\chi^2$  minimization, leaving as free parameters the intensity, scale radius and peak position. The choice of a particular model for the line surface brightness distribution does not affect the final BH mass estimate provided that the model reproduces the observed line emission within the errors. Nevertheless it has an important effect on the quality of the velocity fit (Marconi et al. 2006).

The  $\chi^2$  reduced values ( $\chi_r^2 = \chi^2/\text{d.o.f.}$ ) of the best fit to the velocity curves, obtained for each disk inclination, are shown in Fig. 9. The quality of the fit depends only very weakly on the assumed disk inclination, with almost constant values of  $\chi_r^2$  up to  $i = 60^\circ$ , while  $\chi_r^2$  rapidly increases at larger inclinations. The overall best fitting model to our data is obtained for  $i = 30^\circ$  for the set of parameters reported in Table 1 and is presented in Fig. 10.

The value of minimum  $\chi_r^2$  is far larger than the value indicative of a good fit and this is in contrast with the fact that the curves shown in Fig. 10 seem to trace the data points well. The reason for this discrepancy is that  $\chi_r^2$  is not properly normalized

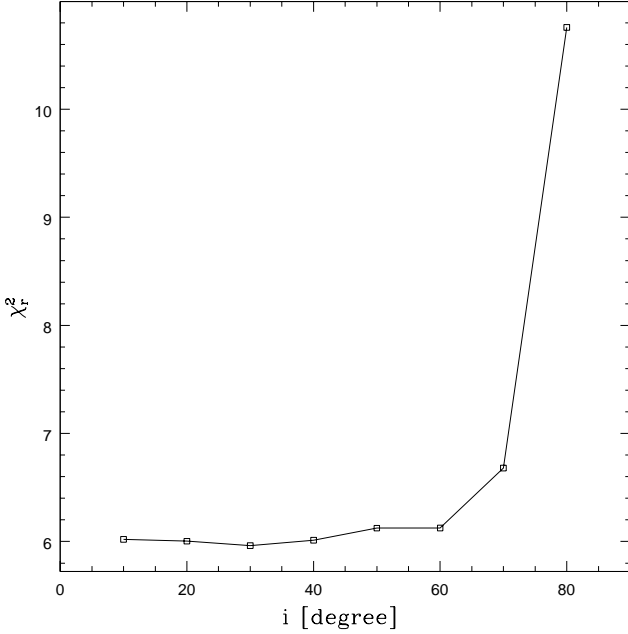


**Fig. 9.**  $\chi_r^2$  values of the best fit obtained for each disk inclination.

**Table 1.** Best fit parameter set

$i$	$b$	$s_0$	$\theta$	$V_{\text{sys}}$	$\Upsilon_V$	$M_{\text{BH}}(M_\odot)$	$\chi_r^2$
30	0.00	-0.02	28	1010	6.5	$2.7 \times 10^8$	5.96

(e.g. because not all points are independent or as they do not include the uncertainties in the relative wavelength calibration for the five slits) and/or imply the presence of small deviations from pure rotation. Following Barth et al. (2001) we then rescaled the error bars in our velocity measurements by adding in quadrature a constant error such that the overall best fitting model provides  $\chi^2/\text{d.o.f.} \sim 1$ . This is a quite conservative approach as it has the effect of increasing the final uncertainty on  $M_{\text{BH}}$ . The additional velocity error is found to be  $28 \text{ km s}^{-1}$ . We rescaled all values of  $\chi_r^2$  with this procedure (Fig. 11, bottom panel). The best fitting models obtained at varying disk inclination are within the  $2\sigma$  confidence level ( $\Delta\chi_r^2 \leq 0.09$ ) for  $10^\circ \leq i \leq 70^\circ$ .

To evaluate the statistical uncertainty associated to the black hole mass estimate we explored its variation with respect to the parameters that are more strongly coupled to it, i.e. the mass-to-light ratio  $\Upsilon_V$  and the gas disk inclination  $i$ . The uncertainty on  $M_{\text{BH}}$  associated to changes in  $\Upsilon_V$  has been estimated building a  $\chi_r^2$  grid in the  $M_{\text{BH}}$  vs.  $\Upsilon_V$  parameter space. At each point of the grid, described by a fixed pair of  $M_{\text{BH}}$  and  $\Upsilon_V$  values, we obtained the best fit model allowing all other parameters to vary freely and derived the corresponding  $\chi_r^2$  value (properly rescaled). This enabled us to build contours of confidence level. The result of this analysis at  $i = 30^\circ$  is presented in Fig. 12. The  $2\sigma$  ranges of the BH mass and mass-to-light ratio at this disk inclination are  $M_{\text{BH}} = 2.7^{+1.5}_{-1.0} \times 10^8 M_\odot$  and  $\Upsilon_V = 6.5^{+5.3}_{-3.0}$  respectively. The statistical uncertainty on  $M_{\text{BH}}$  is reported in the error bar in Fig. 11. We repeated the same analysis for another representative value of the inclination,  $60^\circ$ , obtaining similar fractional uncertainties on the parameters.

The dependence of BH mass on the gas disk inclination closely follows the expected scaling with a  $\propto 1/\sin^2 i$  law (see Fig. 11), at least up to  $i \leq 60^\circ$ . Since all disk inclination

$i \leq 70^\circ$  yield acceptable fits (within the  $2\sigma$  level), apparently our analysis only provides a lower bound to the black-hole mass. However, also the mass-to-light ratio  $\Upsilon_V$  increases sharply at low inclinations reaching a value of 50 for  $i = 10^\circ$ . In fact at smaller inclinations a deeper potential is needed to maintain the projected velocities seen at the largest radii where the stellar component dominates. We then considered the evolutionary synthesis models for stellar populations derived by Maraston (1998) in order to limit ourselves only to astrophysically acceptable models. The value of  $\Upsilon_V$  monotonically increases with the galaxy's age reaching, for a Salpeter initial mass function (IMF), the maximum value in the V band of  $\Upsilon_V = 7.87$  for an age of 15 Gyr. This value corresponds to an inclination of  $\sim 27^\circ$  (having used a  $1/\sin^2 i$  interpolation on the disk inclination for the dependence of both  $\Upsilon_V$  and  $M_{\text{BH}}$ ). This translates into an upper bound to the black hole mass (see Fig. 11). Therefore, although larger black-hole masses are allowed when considering only the kinematical modeling, they are in reality unacceptable as they would correspond to a mass-to-light ratio of the stellar population larger than predicted by the stellar population synthesis. Furthermore, the adopted upper limit on  $\Upsilon_V$  compares favourably with observations. The correlation between galaxy's luminosity and mass-to-light ratio (e.g. van der Marel 1991; Cappellari et al. 2006) predicts a range (in the R band) of  $\Upsilon_R \sim 3 - 6.5$ . This is consistent with an age of 7 - 15 Gyr and with the upper limit we adopted in the V band.

By combining the allowed range in inclination with the statistical uncertainties on  $M_{\text{BH}}$  associated to variations in  $\Upsilon_V$ , we obtain a global range of acceptable black hole mass of  $M_{\text{BH}} = (0.7 - 5.1) \times 10^8 M_\odot$  at a  $2\sigma$  level.

#### 4.2.1. Line width distribution

At this point of our analysis we tested the influence over the above results of including the line width in the fitting procedure. Adopting the best fit parameter set (Table 1) we obtained the FWHM distribution shown in Fig. 13 (solid line). The observed line widths are acceptably well reproduced by the model. Only a slightly underestimate ( $\sim 20\%$ ) of the nuclear increase is observable at NUC, while the largest deviation from the peak values occurs at the off-nuclear S1. Among the line parameters, the line width is the most sensitive to the brightness distribution modeling and to other computational problems, i.e. a sub-sampling of the grid used by the numerical code (Marconi et al. 2006). Due to this sensitivity only weak constraints on the BH mass estimate can be derived by its inclusion in the fitting procedure. Therefore, a slightly underestimate of the peak observed values does not invalidate the derived fitting model.

Despite the goodness of the result, we repeated the  $\chi^2$  minimization at  $i = 30^\circ$ , this time by including the observed line widths in the modeling procedure. The best fit obtained is shown in Fig. 13 (dashed line). Only a small improvement of the match with observed values is obtained, while the model velocity curves remain substantially unchanged respect to the previous result. Furthermore, BH mass and mass-to-light ratio values do not change significantly, resulting  $M_{\text{BH}} = 3.1 \times 10^8 M_\odot$  and  $\Upsilon_V = 5.6$ . The modeling code assumption that the nuclear gas is in a thin, circularly rotating disk is then verified through the satisfactory good match of observed and model line width distributions. Indeed, the nuclear rise of the line width is well accounted for as unresolved rotation by the fitting model.

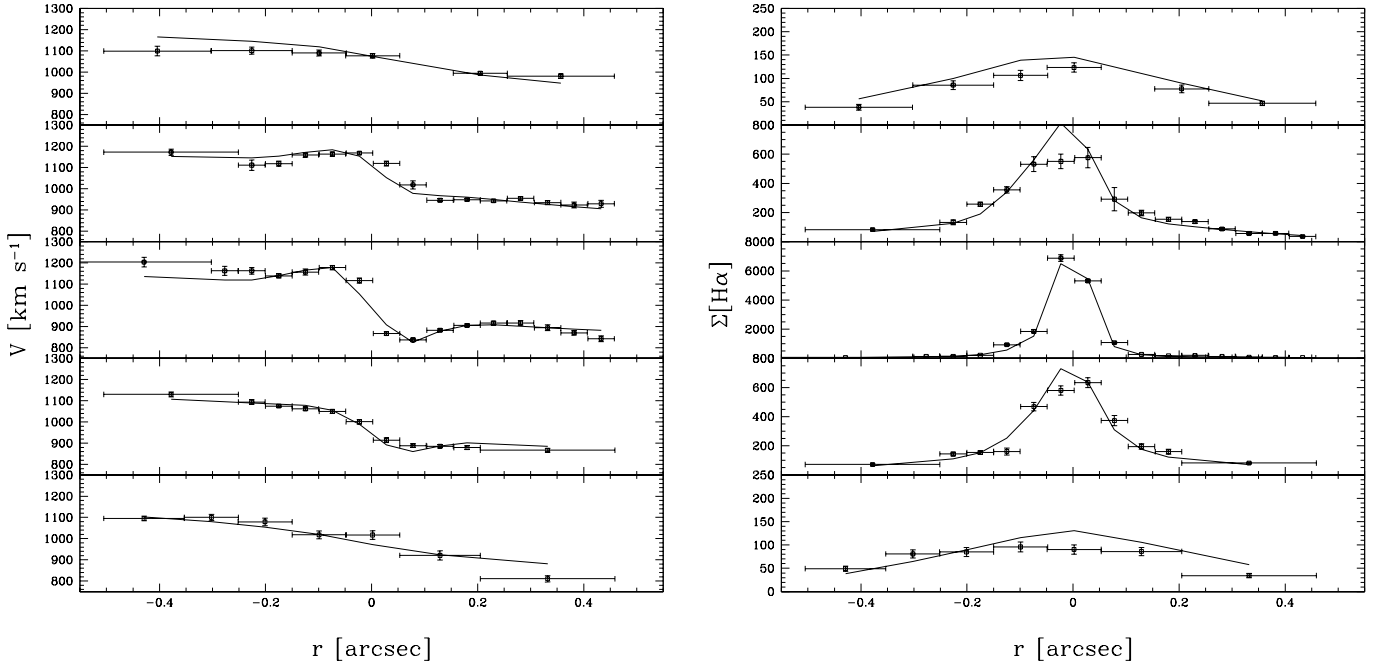


**Fig. 10.** Overall best fit to the rotation curves (left), assumed line surface brightness distribution (right). From upper to bottom panel: N2, N1, NUC, S1 and S2.

## 5. Discussion

Our model fitting of the nuclear rotation curves of NGC 3998 indicates that the kinematics of gas in its innermost regions can be successfully accounted for by circular motions in a thin disk when a point-like dark mass (presumably a supermassive black hole) of  $M_{\text{BH}} = 2.7^{+2.4}_{-2.0} \times 10^8 M_{\odot}$  is added to the galaxy potential.

Let us explore how this mass determination is connected with the properties of the host galaxy. We compare our BH mass estimate with the known correlations with host spheroid (bulge) mass (Marconi & Hunt 2003) and with the stellar velocity dispersion (Tremaine et al. 2002; Ferrarese & Ford 2005).

Following Marconi & Hunt (2003), we used the virial mass ( $M_{\text{vir}} = 3R_e\sigma_{\text{bul}}^2/G$ ) to determine the bulge mass of NGC 3998.

The effective radius of the bulge,  $R_e$ , has been estimated as the weighted average of the determinations by Fisher et al. (1996) ( $11''$ ) and Sánchez-Portal et al. (2004) ( $9''.6$ ), from which we derived  $R_e = 10''.2 \pm 0''.6$  ( $0.85 \pm 0.05$  kpc).

We found three optical determinations of the stellar velocity dispersion for NGC 3998 in the literature. The values are  $297 \text{ km s}^{-1}$  (Fisher 1997,  $2'' \times 4''$  slit),  $314 \pm 20 \text{ km s}^{-1}$  (Tonry & Davis 1981,  $3'' \times 12''$  slit),  $333 \pm 22 \text{ km s}^{-1}$  (Nelson & Whittle 1995,  $1''.5 \times 2''.2$  slit) respectively<sup>2</sup>. We adopted the value from HyperLeda database  $\sigma_{\text{star}} = (305 \pm 10) \text{ km s}^{-1}$ . The velocity dispersions in the catalogue are mean values standardized to a circular aperture of radius  $r_{\text{ap}} = 0.595 \text{ h}^{-1} \text{ kpc}$  (see Golev & Prugniel 1998). At the distance of NGC 3998 this radius corresponds to an aperture of  $9''.6$  of radius, very close to the value of the bulge effective radius for NGC 3998.

Assuming that this value of  $\sigma_{\text{star}}$  is a good approximation for  $\sigma_{\text{bul}}$ , we obtained for the bulge mass the value  $M_{\text{bul}} = (5.5 \pm 0.7) \times 10^{10} M_{\odot}$ . Using this estimate of  $M_{\text{bul}}$  and the corre-

<sup>2</sup> Bertola et al. (1984) measured  $\sigma = 350 \pm 40 \text{ km s}^{-1}$ , but, because of saturation, their data gave no results on stellar kinematics in the innermost central regions ( $< 2''$ ).

lation of Marconi & Hunt (2003) which considers only “secure” BH mass determinations (i.e. BH with resolved sphere of influence:  $2R_{\text{sph}}/R_{\text{res}} > 1$ , with  $R_{\text{res}}$  the spatial resolution of the observations) the expected  $M_{\text{BH}}$  for NGC 3998 is  $1.3 \times 10^8 M_{\odot}$ , in excellent agreement, within a factor of 2, with our determination (see Fig. 14). We also note that the value of the BH sphere of influence radius in NGC 3998 ( $R_{\text{sph}} = GM_{\text{BH}}/\sigma_{\text{star}}^2$ ) is  $R_{\text{sph}} \sim 13 \text{ pc}$  ( $0''.16$ ). This implies a well resolved BH sphere of influence at the HST resolution ( $\sim 0''.1$ ) for our  $M_{\text{BH}}$  determination ( $2R_{\text{sph}}/R_{\text{res}} \approx 3.2$ ).

Concerning the correlations between BH mass and central stellar velocity dispersion, adopting the correlation parameters estimated by Tremaine et al. (2002) the expected BH mass for NGC 3998 is  $7.4 \times 10^8 M_{\odot}$  (see Fig. 15), a factor  $\sim 2.7$  higher than our estimate. However, NGC 3998 cannot be considered as an outlier from the  $M_{\text{BH}}$  vs.  $\sigma$  correlation given the errors in the estimates of  $M_{\text{BH}}$ ,  $\sigma_{\text{star}}$ , and of the best fit parameters describing  $M_{\text{BH}} - \sigma$  relation, and its intrinsic scatter ( $0.25 - 0.3$  in  $\log M_{\text{BH}}$ ). We can also compare our measurement with the expectations of the  $M_{\text{BH}} - \sigma$  relation recently derived by Ferrarese & Ford (2005). We then normalized the central velocity dispersion to an aperture of radius equal to  $1/8$  of  $R_e$ , following the method introduced by Jorgensen et al. (1995), and derived  $\sigma_{R_e/8} = 330 \pm 11 \text{ km s}^{-1}$ . This form of the correlation predicts a BH mass of  $1.9 \times 10^9 M_{\odot}$ , a factor of 7 higher than our estimate, a larger discrepancy than the one found adopting the Tremaine et al. values.

Marconi & Hunt (2003) showed with a partial correlation analysis that  $M_{\text{BH}}$  is separately significantly correlated both with  $\sigma$  and  $R_e$ . This is clearly shown by the residuals of the  $M_{\text{BH}} - \sigma$  correlation against  $R_e$  that show a weak, but significant, correlation (reproduced here in Fig. 16). The new measurement of the black hole mass in NGC 3998 supports this idea. In fact, NGC 3998 has one of the smallest values of  $R_e$  among galaxies with measured  $M_{\text{BH}}$  ( $0.85 \text{ kpc}$ ) and it shows a negative residual from the  $M_{\text{BH}} - \sigma$  correlation. Recently Capetti et al. (2005) found a



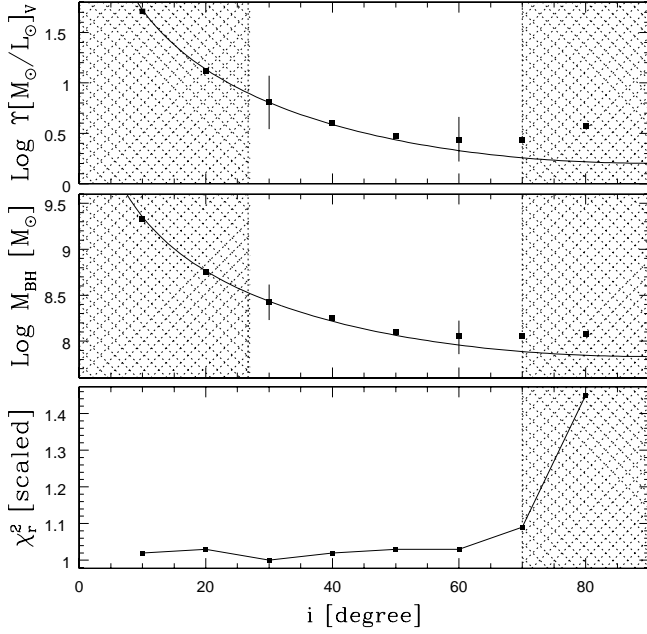


**Fig. 11.** Best fit values of  $\gamma_V$  and  $M_{\text{BH}}$  obtained by varying the disk inclination  $i$  (upper and middle panels). The corresponding  $\chi_r^2$  are shown in the bottom panel. The lines in the upper and middle panels reproduce the  $\propto 1/\sin^2 i$  dependence of  $M_{\text{BH}}$  and  $\gamma_V$ . Inclinations larger than  $70^\circ$  are excluded at a confidence level of  $2\sigma$  (shaded region in the right side of the diagrams). Models with inclinations smaller than  $27^\circ$  are excluded since they correspond to unacceptably high values of  $\gamma_V$  (shaded region in the left side of the diagrams, bounded by  $\gamma_V = 7.87$  as expected for a Salpeter IMF).

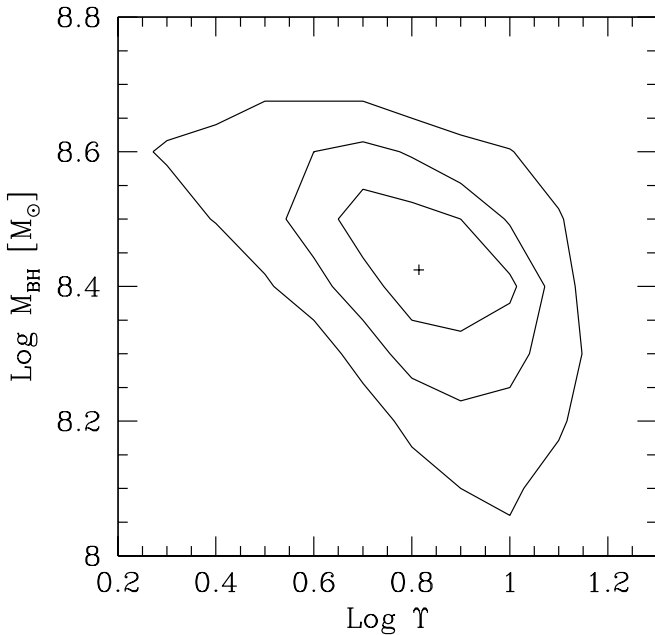


**Fig. 12.**  $\chi_r^2$  contours at varying  $\gamma_V$  and  $M_{\text{BH}}$  at an inclination of  $i = 30^\circ$ . Contours are plotted for confidence levels of 1, 2 and 3  $\sigma$ . The plus sign marks the overall best fit.

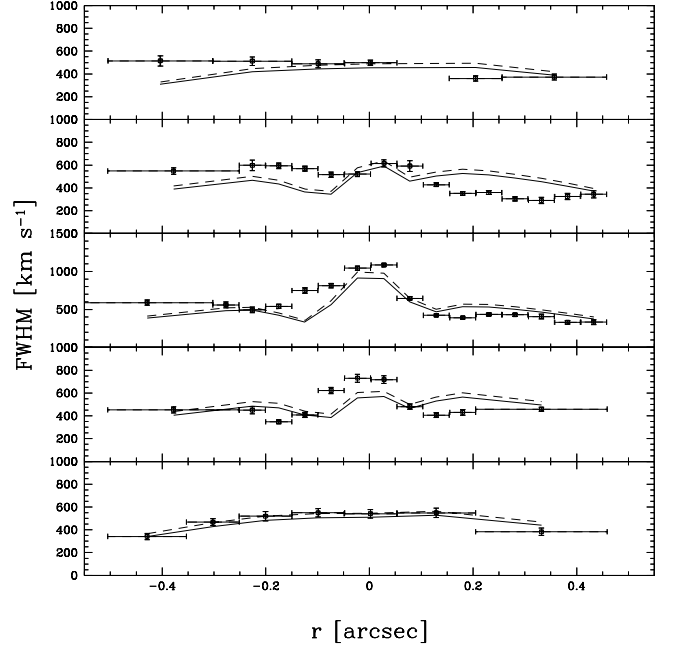


**Fig. 13.** Line width distribution expected from the overall best fit model (solid line) at  $i = 30^\circ$ , and derived (dashed line) by including the observed line widths in the fitting procedure. From upper to bottom panel: N2, N1, NUC, S1 and S2.

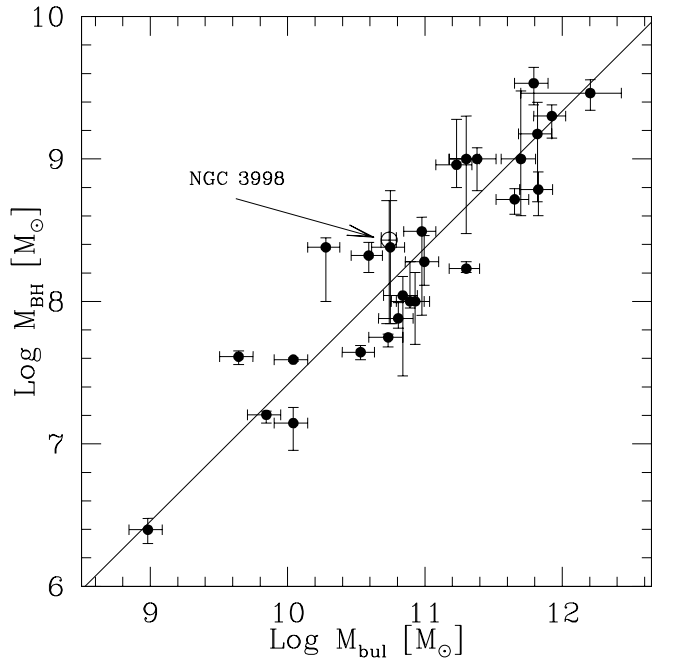


**Fig. 14.**  $M_{\text{BH}}$  vs bulge mass from Marconi & Hunt (2003) with the best fit obtained from a bisector linear regression analysis (solid line). The position of NGC 3998 (empty circle) is indicated by an arrow.

similar result, but in the opposed sense, considering the Seyfert galaxy NGC 5252: a large effective radius (9.7 kpc) corresponds in this galaxy to a large positive residual. This confirms that a combination of both  $\sigma$  and  $R_e$  is necessary to drive the correla-

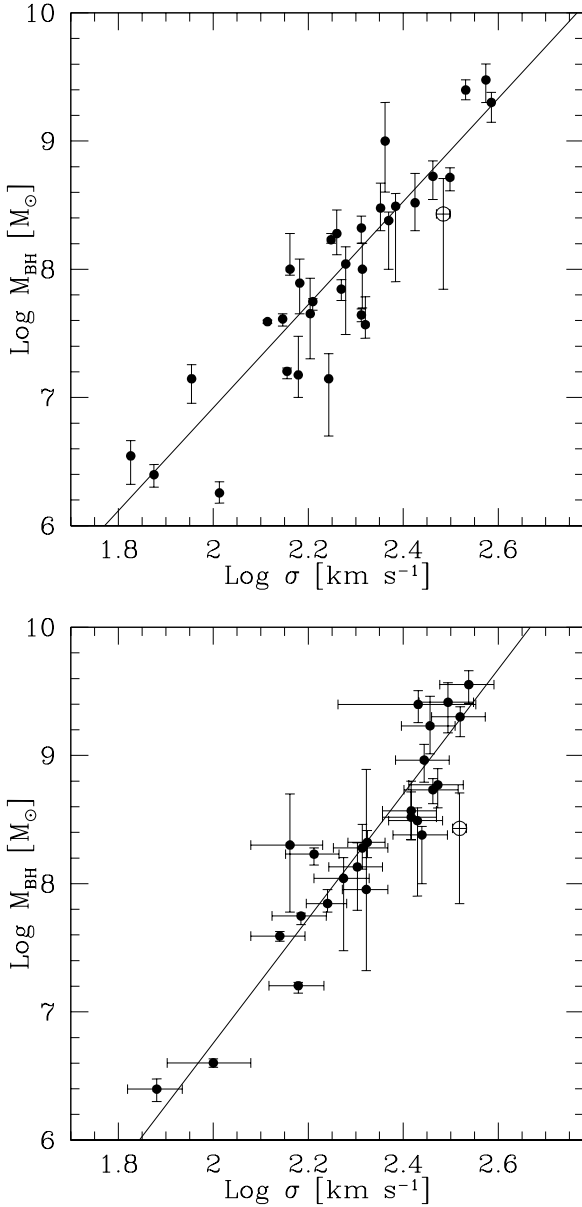


**Fig. 15.**  $M_{\text{BH}}$  vs central stellar velocity dispersion from Tremaine et al. (2002) (upper panel) and from Ferrarese & Ford (2005) (lower panel). Solid lines indicate the best fits for the two correlations. The position of NGC 3998 is shown by an empty circle.

tions between  $M_{\text{BH}}$  and other bulge properties, an indication for the presence of a black holes “fundamental plane”.

## 6. Summary and conclusions

We have presented results from a gas kinematics study in the nucleus of the nearby S0 active galaxy NGC 3998. The analyzed data were retrieved from archival HST/STIS long-slit spectra. We performed an analysis of the  $\text{H}\alpha$ ,  $[\text{N II}]\lambda\lambda 6548, 6583$  and  $[\text{S II}]\lambda\lambda 6716, 6731$  emission lines profiles to derive the map of the gas velocity field. The nuclear velocity curves show a general reflection symmetry and are consistent with the presence of gas in regular rotation. We used our modeling code to fit the observed  $\text{H}\alpha$  surface brightness distribution and velocity curve. The dynamics of the rotating gas can be accurately repro-

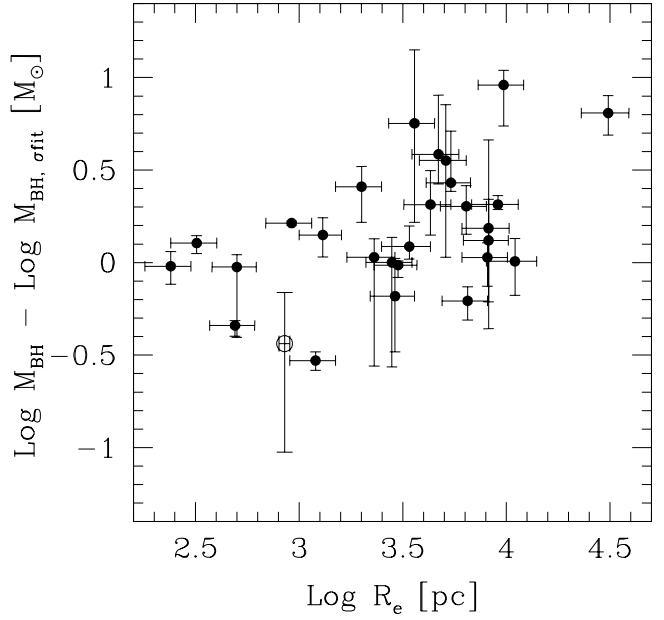


**Fig. 16.** Residuals from the  $M_{\text{BH}}$  vs  $\sigma$  correlation (in the Tremaine’s et al. form) reported against the galaxy’s effective radius  $R_e$ . The position of NGC 3998 is indicated by an empty circle.

duced by motions in a thin disk when a compact dark mass of  $M_{\text{BH}} = 2.7_{-2.0}^{+2.4} \times 10^8 M_{\odot}$ , very likely a supermassive black hole, is added to the stellar mass component. This result is also supported by the satisfactory good match of observed and model line width distributions. Furthermore, the black hole in NGC 3998 has a sphere of influence radius of  $\sim 13$  pc ( $0''.16$ ). At the high HST spatial resolution, this value of  $R_{\text{sph}}$  implies a resolved BH sphere of influence for our  $M_{\text{BH}}$  determination ( $2R_{\text{sph}}/R_{\text{res}} \simeq 3.2$ ).

For what concerns the connections of this BH mass estimate with the properties of the host galaxy, the  $M_{\text{BH}}$  value for NGC 3998 is in excellent agreement (within a factor of 2) with the  $M_{\text{BH}} - M_{\text{bul}}$  correlation between BH and host bulge mass. The black hole mass predicted by the  $M_{\text{BH}} - \sigma_{\text{bul}}$  correlation is a factor of 2.7 larger than our measure, adopting the relation found by Tremaine et al. (2002), or a factor of 7 using the most recent parameterization by Ferrarese & Ford (2005). However, NGC 3998 cannot be considered as an outlier from the  $M_{\text{BH}}$  vs.  $\sigma$  correlation considering the errors in the estimates of  $M_{\text{BH}}$  and  $\sigma_{\text{star}}$ , and both the uncertainties in the determination of the  $M_{\text{BH}} - \sigma$  relation as well as its scatter.

Nonetheless, the lower-than-expected value for the mass of the black hole hosted by NGC 3998 strengthens the presence of a connection between the residuals from the  $M_{\text{BH}} - \sigma$  relation and the galaxy’s effective radius. In fact, NGC 3998 has one of the smallest values of  $R_e$  among galaxies with measured  $M_{\text{BH}}$  and it shows a negative residual. We also recently showed that the opposite is true for the Seyfert galaxy NGC 5252: a large effective radius corresponds in this galaxy to a large positive residual.

Apparently only with a combination of both  $\sigma$  and  $R_e$  it is possible to account for the correlations between  $M_{\text{BH}}$  and other bulge properties, an indication for the presence of a black holes “fundamental plane”. Clearly, only by further increasing

the number of direct black hole measurements it will be possible to base these conclusions on a stronger statistical foundation.

*Acknowledgements.* We would like to thank the referee, Laura Ferrarese, for her useful comments and suggestions.

## References

- Bahcall, J. N. & Wolf, R. A. 1976, *ApJ*, 209, 214  
 Barth, A. J., Filippenko, A. V., & Moran, E. C. 1999, *ApJ*, 525, 673  
 Barth, A. J., Ho, L. C., Filippenko, A. V., & Sargent, W. L. W. 1998, *ApJ*, 496, 133  
 Barth, A. J., Sarzi, M., Rix, H., et al. 2001, *ApJ*, 555, 685  
 Bertola, F., Bettoni, D., Rusconi, L., & Sedmak, G. 1984, *AJ*, 89, 356  
 Braatz, J. A., Wilson, A. S., & Henkel, C. 1997, *ApJS*, 110, 321  
 Capetti, A., Marconi, A., Macchetto, D., & Axon, D. 2005, *A&A*, 431, 465  
 Cappellari, M., Bacon, R., Bureau, M., et al. 2006, *MNRAS*, 366, 1126  
 Chokshi, A. & Turner, E. L. 1992, *MNRAS*, 259, 421  
 Dressler, A. & Richstone, D. O. 1988, *ApJ*, 324, 701  
 Erwin, P., Graham, A. W., & Caon, N. 2004, in *Coevolution of Black Holes and Galaxies*, ed. L. C. Ho  
 Fabbiano, G., Fassnacht, C., & Trinchieri, G. 1994, *ApJ*, 434, 67  
 Ferrarese, L. & Ford, H. 2005, *Space Science Reviews*, 116, 523  
 Ferrarese, L., Ford, H. C., & Jaffe, W. 1996, *ApJ*, 470, 444  
 Ferrarese, L. & Merritt, D. 2000, *ApJ*, 539, L9  
 Filho, M. E., Barthel, P. D., & Ho, L. C. 2002, *A&A*, 385, 425  
 Fisher, D. 1997, *AJ*, 113, 950  
 Fisher, D., Franx, M., & Illingworth, G. 1996, *ApJ*, 459, 110  
 Gebhardt, K., Bender, R., Bower, G., et al. 2000, *ApJ*, 539, L13  
 Golev, V. & Prugniel, P. 1998, *A&AS*, 132, 255  
 González Delgado, R. M., Cid Fernandes, R., Pérez, E., et al. 2004, *ApJ*, 605, 127  
 Graham, A. W., Erwin, P., Caon, N., & Trujillo, I. 2001, *ApJ*, 563, L11  
 Haehnelt, M. G. & Kauffmann, G. 2000, *MNRAS*, 318, L35  
 Häring, N. & Rix, H.-W. 2004, *ApJ*, 604, L89  
 Harms, R. J., Ford, H. C., Tsvetanov, Z. I., et al. 1994, *ApJ*, 435, L35  
 Heckman, T. M. 1980, *A&A*, 87, 152  
 Ho, L. C., Filippenko, A. V., & Sargent, W. L. W. 1997a, *ApJS*, 112, 315  
 Ho, L. C., Filippenko, A. V., Sargent, W. L. W., & Peng, C. Y. 1997b, *ApJS*, 112, 391  
 Hummel, E., van der Hulst, J. M., & Dickey, J. M. 1984, *A&A*, 134, 207  
 Jorgensen, I., Franx, M., & Kjaergaard, P. 1995, *MNRAS*, 276, 1341  
 Keel, W. C. 1983, *ApJ*, 269, 466  
 Koratkar, A., Deustua, S. E., Heckman, T., et al. 1995, *ApJ*, 440, 132  
 Kormendy, J. & Gebhardt, K. 2001, in *AIP Conf. Proc. 586: 20th Texas Symposium on relativistic astrophysics*, ed. J. C. Wheeler & H. Martel, 363  
 Kormendy, J. & Richstone, D. 1995, *ARA&A*, 33, 581  
 Lynden-Bell, D. 1969, *Nature*, 223, 690  
 Macchetto, F., Marconi, A., Axon, D. J., et al. 1997, *ApJ*, 489, 579  
 Magorrian, J., Tremaine, S., Richstone, D., et al. 1998, *AJ*, 115, 2285  
 Maoz, D., Filippenko, A. V., Ho, L. C., et al. 1995, *ApJ*, 440, 91  
 Maoz, D., Nagar, N. M., Falcke, H., & Wilson, A. S. 2005, *ApJ*, 625, 699  
 Maraston, C. 1998, *MNRAS*, 300, 872  
 Marconi, A., Axon, D. J., Capetti, A., et al. 2003, *ApJ*, 586, 868  
 Marconi, A. & Hunt, L. K. 2003, *ApJ*, 589, L21  
 Marconi, A., Pastorini, G., Pacini, F., et al. 2006, *A&A*, 448, 921  
 Marconi, A., Risaliti, G., Gilli, R., et al. 2004, *MNRAS*, 351, 169  
 McLure, R. J. & Dunlop, J. S. 2002, *MNRAS*, 331, 795  
 Merritt, D. & Ferrarese, L. 2001, in *ASP Conf. Ser. 249: The Central Kiloparsec of Starbursts and AGN: The La Palma Connection*, ed. J. H. Knapen, J. E. Beckman, I. Shlosman, & T. J. Mahoney, 335  
 Nagar, N. M., Falcke, H., Wilson, A. S., & Ulvestad, J. S. 2002, *A&A*, 392, 53  
 Nelson, C. H. & Whittle, M. 1995, *ApJS*, 99, 67  
 Pellegrini, S., Cappi, M., Bassani, L., della Ceca, R., & Palumbo, G. G. C. 2000, *A&A*, 360, 878  
 Pogge, R. W., Maoz, D., Ho, L. C., & Eracleous, M. 2000, *ApJ*, 532, 323  
 Press, W. H., Teukolsky, S. A., Vetterling, W. T., & Flannery, B. P. 1992, *Numerical recipes in FORTRAN. The art of scientific computing* (Cambridge: University Press, c1992, 2nd ed.)  
 Roberts, T. P. & Warwick, R. S. 2000, *MNRAS*, 315, 98  
 Salpeter, E. E. 1964, *ApJ*, 140, 796  
 Sánchez-Portal, M., Díaz, Á. I., Terlevich, E., & Terlevich, R. 2004, *MNRAS*, 350, 1087  
 Schmidt, M. 1963, *Nature*, 197, 1040  
 Sérsic, J.-L. 1968, *Atlas de Galaxias Australes*(Córdoba: Obs. Astron.)  
 Shankar, F., Salucci, P., Granato, G. L., De Zotti, G., & Danese, L. 2004, *MNRAS*, 354, 1020  
 Silk, J. & Rees, M. J. 1998, *A&A*, 331, L1  
 Soltan, A. 1982, *MNRAS*, 200, 115  
 Tonry, J. L. & Davis, M. 1981, *ApJ*, 246, 666  
 Tremaine, S., Gebhardt, K., Bender, R., et al. 2002, *ApJ*, 574, 740  
 Valluri, M., Merritt, D., & Emsellem, E. 2004, *ApJ*, 602, 66  
 van der Marel, R. P. 1991, *MNRAS*, 253, 710  
 van der Marel, R. P., Cretton, N., de Zeeuw, P. T., & Rix, H.-W. 1998, *ApJ*, 493, 613  
 van der Marel, R. P. & van den Bosch, F. C. 1998, *AJ*, 116, 2220  
 Verolme, E. K., Cappellari, M., Copin, Y., et al. 2002, *MNRAS*, 335, 517  
 Yu, Q. & Tremaine, S. 2002, *MNRAS*, 335, 965

## Appendix A: Fitting parameters for STIS spectra.

### List of Objects

‘NGC 3998’ on page 1

**Table A.1.** Fitting parameters for the narrow emission line spectra at each location (x coord.) along the slit. The relative flux of the [NII] lines was held fixed to 0.334, so only the [NII] $\lambda$ 6583 is listed. From upper to bottom table: NUC, N1, S1, N2 and S2 positions.

$x$	$V$	$dV$	$FWHM$	$dFWHM$	$\Sigma(H\alpha)$	$d\Sigma(H\alpha)$	$\Sigma(NII)$ ( $\lambda$ 6583)	$d\Sigma(NII)$ ( $\lambda$ 6583)	$\Sigma(SII)$ ( $\lambda$ 6716)	$d\Sigma(SII)$ ( $\lambda$ 6716)	$\Sigma(SII)$ ( $\lambda$ 6731)	$d\Sigma(SII)$ ( $\lambda$ 6731)
591-595	1204	23	590	35	61	7	77	6	25	5	24	6
596	1163	21	561	39	135	16	161	13	42	10	63	11
597	1163	16	495	38	143	24	198	24	89	9	77	10
598	1139	11	541	29	208	26	288	25	142	10	150	11
599	1157	14	750	37	934	71	1060	72	262	25	347	30
600	1178	10	814	30	1853	109	2257	113	577	32	701	40
601	1117	13	1044	28	6873	230	6210	168	883	78	1647	93
602	867	8	1085	23	5315	107	4187	94	766	31	1096	37
603	837	8	646	21	1081	55	1140	51	311	16	387	20
604	882	6	422	16	269	25	325	20	158	8	156	10
605	905	7	391	16	169	18	224	15	117	7	129	9
606	917	8	434	18	200	14	220	12	107	8	110	9
607	917	10	431	21	134	11	150	10	79	6	80	8
608	894	14	407	32	82	9	93	6	44	7	41	8
609	870	11	331	23	67	8	78	8	39	5	37	6
610	842	14	333	32	51	8	54	7	39	5	16	6
592-596	1172	15	548	29	83	6	387	5	167	4	152	5
597	1111	24	598	46	133	17	161	13	43	11	59	12
598	1118	12	594	24	257	15	268	12	65	9	92	10
599	1159	10	569	22	356	22	421	22	131	9	184	11
600	1163	9	516	24	532	51	553	41	172	15	216	18
601	1168	8	521	21	551	49	622	40	215	13	251	15
602	1119	12	615	32	576	70	585	53	214	12	211	14
603	1018	20	592	47	292	80	396	57	195	12	194	15
604	946	7	428	16	197	18	251	16	124	7	145	9
605	948	6	351	15	154	14	162	12	99	6	86	7
606	942	7	359	18	137	11	162	10	77	7	77	8
607	954	7	304	18	88	8	99	7	62	5	64	6
608	935	9	289	27	57	8	80	8	35	5	48	6
609	923	14	325	28	57	8	61	7	29	5	10	5
610	929	16	344	31	36	6	46	6	21	4	28	5
592-596	1130	11	453	27	72	6	76	5	39	4	32	4
597	1094	12	450	32	145	13	140	20	54	8	65	9
598	1075	6	348	17	154	11	183	9	56	7	88	8
599	1062	9	409	23	161	24	231	20	98	8	125	10
600	1050	10	622	27	469	29	476	28	134	11	192	13
601	1001	11	730	35	580	32	657	34	149	12	222	15
602	914	11	718	33	633	35	629	34	144	13	226	16
603	888	9	481	24	373	36	328	28	123	9	116	10
604	885	8	406	21	196	19	214	17	108	7	77	8
605	879	10	431	25	160	17	170	16	87	8	62	9
606-610	867	8	458	17	82	5	92	5	45	3	46	4
592-595	1099	22	515	45	38	6	58	5	12	4	15	5
596-598	1101	17	512	37	86	9	94	7	34	6	45	6
599-600	1090	14	489	35	106	11	134	9	33	6	60	8
601-602	1077	11	498	24	123	10	166	9	48	6	63	7
605-606	994	9	360	23	78	8	110	7	38	5	48	6
607-610	980	11	372	26	46	5	53	5	23	3	31	4
592-594	1095	11	342	27	49	6	50	4	24	3	28	4
595-596	1100	15	468	30	81	9	85	7	38	5	39	6
597-598	1079	18	519	41	85	10	95	8	35	6	24	7
599-600	1018	19	549	37	96	11	115	9	38	6	41	7
601-602	1017	20	541	37	90	10	97	8	30	5	37	7
603-605	921	21	548	41	86	9	81	7	29	5	27	6
606-610	811	15	383	33	34	5	42	4	16	3	18	3